Iranian Journal of Geophysics, Vol 20 No 6, 2027, Page 129 – 145 (Research Article)
DOI: 10.30499/ijg.2025.526698.1705

Seismic vulnerability and sediment thickness assessment using HVSR in Musi Banyuasin district, south Sumatra

Agustya Adi Martha[1], Dwi Miftahuljanah.S[2], Nurul Hudayat[3*], Moh Sarkowi[4] and Tio Azhar Prakoso Setiadi[5]

[1] Associate Professor, National Research and Innovation Agency, Bogor, Indonesia
[2] Bachelor, Geophysical Engineering, Universitas Lampung, Sumantri Brojonegoro Lampung, Indonesia
[3] M.Sc., National Research and Innovation Agency, Bogor, Indonesia
[4] Professor,Geophysical Engineering, Universitas Lampung, Sumantri Brojonegoro Lampung, Indonesia
[5] Bachelor, National Research and Innovation Agency, Bogor, Indonesia

(Received: 03 June 2025, Accepted: 30 September 2025)

Abstract

Indonesia, located at the convergence of active tectonic plates, is highly susceptible to earthquakes. Musi Banyuasin District in South Sumatra is one of the regions characterized by complex geological structures and potential seismic hazards. This study investigates sediment thickness and seismic vulnerability index as key parameters for evaluating local site effects. The Horizontal to Vertical Spectral Ratio (HVSR) method was applied to analyze dominant frequency (f_0), amplification factor (A_0), dominant period (T_0), seismic vulnerability index (Kg), and sediment thickness (H). The results show that dominant frequency ranges from 2 to 18 Hz, amplification values vary between 1.6 and 5.2, dominant period spans 0.04–0.38 s, seismic vulnerability index ranges from 0.2 to 3.2, and sediment thickness varies from 8 to 64 m. The majority of the study area is classified as type I soil with hard rock formations based on frequency and period parameters. Overall, the low amplification and seismic vulnerability index values indicate a relatively minimal potential for severe earthquake damage. These findings provide new insights into the subsurface conditions of Musi Banyuasin and highlight their relevance for disaster risk reduction. The results can serve as a scientific basis for future land-use planning and construction strategies aimed at mitigating seismic risk in the region.

Keywords: HVSR, Musi Banyuasin, earthquake, local site effect, mitigation

*Corresponding author: nurul.hudayat@brin.go.id

1 Introduction

Indonesia is located at the intersection of three active tectonic plates: the Eurasian Plate, the Indo-Australian Plate, and the Pacific Plate. The western part of Indonesia, particularly along the island of Sumatra, is where the Eurasian Plate and the Indo-Australian Plate interact, extending from the west of Sumatra Island to the south of Java Island and into Nusa Tenggara (Supartoyo & Abdurahman, 2008). Indonesia's geographic location at the convergence of these three plates is one of the main reasons the country is prone to significant earthquake activity (Irsyam et al., 2010). Earthquakes are a frequent natural disaster in Indonesia, as the country lies on the Pacific Ring of Fire, an area known for high seismic and volcanic activity (Lovett, 2006).Although earthquakes are natural events that cannot be accurately predicted in terms of time, location, or intensity, they remain a major concern due to the severe damage they can cause and the potential for loss of life.

One of the areas particularly vulnerable to the impacts of earthquakes is Musi Banyuasin District in South Sumatra Province. This district is located in a region rich in geological diversity, and geologically, it is part of the Sumatra Back-Arc Fold Belt, which is influenced by the complex tectonic activity of the South Sumatra Basin (Barber et al., 2005).The geology of Musi Banyuasin is predominantly composed of sedimentary rocks, including sandstone, shale, and limestone. These formations are the result of sediment deposition from land erosion and volcanic activity in the ocean, rivers, and lakes over long geological periods. Although the region does not have active volcanoes, its location within the Pacific Ring of Fire means it is affected by plate movements that can trigger significant earthquakes. The subduction of the Indo-Australian Plate beneath the Eurasian Plate, along with lateral movement along the Sumatra Fault, creates complex geological structures in this region. These processes have led to the formation of various basins along Sumatra Island, including the South Sumatra Basin, which is a key feature of Musi Banyuasin's geology (Barber et al., 2005).

Previous studies in South Sumatra have highlighted local geological and seismic phenomena. For example, Setiadi et al. (2010) used gravity methods to identify the basin configuration in South Sumatra, providing insights into anomaly depth and geological structure. Maulidah and Santosa (2016) relocated earthquakes in South Sumatra using the Double Difference method, which refined epicenter coordinates and hypocenter depths. More recently, Hadi et al. (2021, 2025) integrated the HVSR method with the Analytical Hierarchy Process to identify earthquake-prone areas in Bengkulu and South Sumatra.

At the national scale, the HVSR method has been widely applied in various regions of Indonesia. Tawakal et al. (2020) conducted HVSR research in East Java, while Minardi et al. (2023) studied Mandalika City. Widia Pamungkas Isburhan et al. (2019) applied HVSR to determine earthquake risk areas in Jakarta City. Hardy et al. (2021) developed the prototype of the Indonesian Seismic Microzonation Information System (Inasmis), which also utilizes outputs from HVSR analysis.

Internationally, HVSR applications have also provided valuable contributions to site-effect studies.

Examples include Zanjan City in Iran (Hakimi et al., 2019), Nanning City in China (Ma & Liao, 2024), Cairo–Suez in Egypt (Salama et al., 2024), Makkah Al-Mukarramah in Saudi Arabia (Abdelrahman et al., 2021), Mfantsiman in Ghana (Miezah-Adams et al., 2024), Querétaro City in Mexico (Zavala et al., 2021), and Turkey (Akkaya, 2020). These studies demonstrate the robustness of the HVSR method in assessing sediment thickness, site response, and their implications for seismic hazard.

Despite these numerous applications, no detailed HVSR-based study has yet been conducted for Musi Banyuasin District, particularly focusing on both sediment thickness and seismic vulnerability index. This research gap is critical, as local site effects associated with sedimentary layers and impedance contrast strongly influence earthquake damage potential (Nakamura, 2000).

Therefore, the aim of this study is to apply the HVSR method to characterize subsurface conditions and quantify seismic parameters, including dominant frequency, amplification factor, dominant period, seismic vulnerability index, and sediment thickness. By mapping these parameters, the research provides critical data for earthquake risk reduction, evidence-based land-use planning, and resilient infrastructure design in Musi Banyuasin District.

1.2 Geology Setting

Banyuasin District, located in South Sumatra Province, Indonesia, lies within the South Sumatra Basin, a region known for its complex geology. The study area is specifically situated in the Air Benakat Formation, a key geological unit composed mainly of sedimentary rocks such as sandstone, claystone, and limestone. This formation, first identified in Air Benakat village, Muara Enim District, spans from the Late Triassic to the Late Miocene and is notable for its high porosity and permeability, making it a major source of oil and natural gas. Besides hydrocarbons, Banyuasin also holds potential coal and gold resources. Geological maps and research locations are detailed in Figures 1 and 2 of the study.

The South Sumatra Basin's stratigraphy is characterized by a large-scale cycle of transgression followed by regression. During the transgression phase, formations such as the Talang Akar, Baturaja, and Gumai Formations (grouped as the Telisa Group) were deposited. The regression phase saw the deposition of the Palembang Group, which includes the Air Benakat Formation where this study is focused, along with the Muara Enim and Kasai Formations. Older formations like the Lemat Formation were laid down before the main transgression event. This stratigraphic framework helps understand the sedimentary history and resource distribution in the basin (Susilawati & Ward, 2006).

1.3 South Sumatra Tectonic

Sumatra Island is situated at the convergence zone between the Indo-Australian Plate and the Eurasian/Sundaland Plate, where the Indo-Australian Plate subducts westward beneath the Eurasian Plate along the Sunda Trench. This tectonic interaction causes significant deformation, including lateral displacement, folding, and faulting, which create complex geological structures such as faults and folds. The island's formation is linked to the collision and suturing of

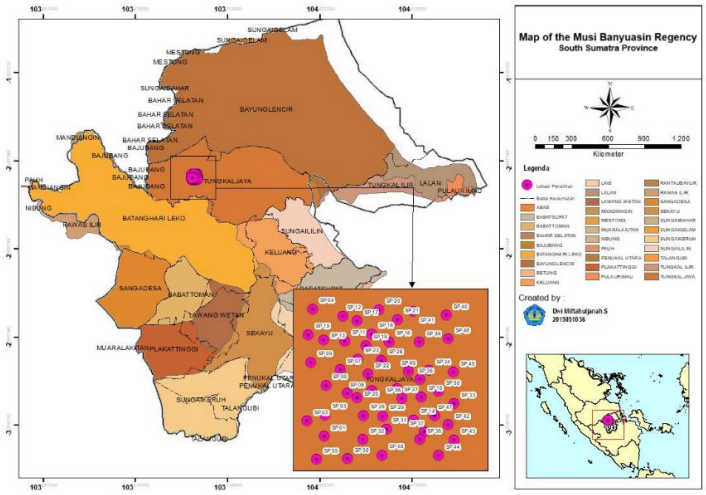

Figure 1. Research Location.

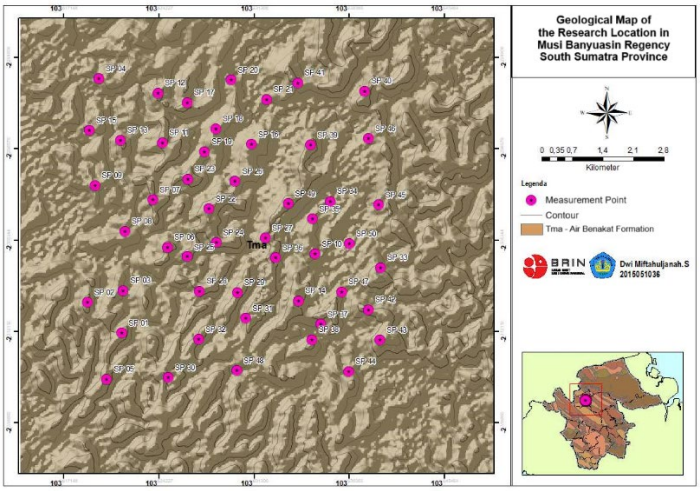

Figure 2. Geological Map of the research location.

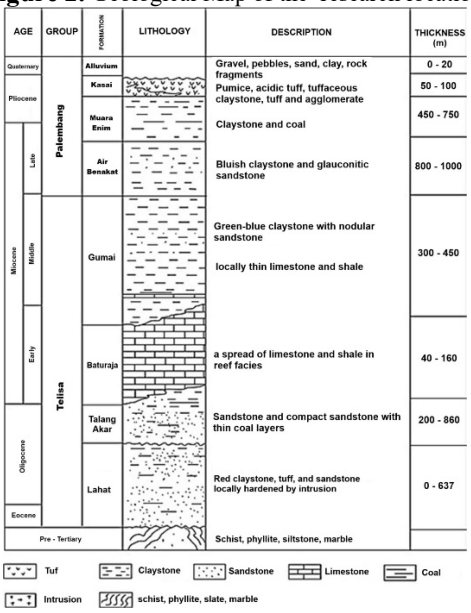

Figure 3. Regional Stratigraphy of the South Sumatra Basin.

microcontinents during the Late Pre-Tertiary period (Barber et al., 2005; Supartoyo & Abdurahman, 2008). Ongoing subduction at a rate of 6 to 7 cm per year drives volcanic activity and metamorphism, producing volcanic materials and metamorphic rocks like granulites. These dynamic geological processes contribute to the South Sumatra Basin's rich natural resources and complex geology.

1.4 Microtremor

Microtremors, or ambient noise, are continuous ground vibrations caused by natural and human activities. Natural sources include wind, earthquakes, ocean waves, and land movements, while human activities such as industrial operations, buildings, and traffic also contribute. The frequency of microtremors varies: low frequencies below 1 Hz mainly come from natural phenomena like ocean waves and atmospheric activity; intermediate frequencies around 0.2 to 0.5 Hz result from ocean wave and shoreline interactions; and higher frequencies above 1 Hz are mostly due to human activities and natural factors like wind and water flow (Takai & Tanaka, 1961). Analyzing microtremors helps reveal subsurface soil properties by studying vibration characteristics, dominant periods, and wave amplification, which are important for understanding soil structure and seismic wave behavior (Nakamura, 2000).

The Horizontal to Vertical Spectral Ratio (HVSR) method is widely used in seismic site characterization by analyzing ambient seismic noise or microtremors. A key parameter is the dominant frequency (f_0), marks the peak in the HVSR curve and reflects the natural resonance of sedimentary layers beneath the site. Its inverse, the dominant period indicates the time during which seismic waves resonate within these layers.

$$T_0 = \frac{1}{f_0} \quad (1)$$

Lower dominant frequencies (longer periods) suggest thicker or softer sediments that amplify seismic waves more, while higher frequencies indicate thinner or stiffer layers. The amplification factor (A_0) measures how much seismic waves are amplified due to contrasts between surface sediments and bedrock, with values A_o and f_o above indicating significant amplification. The seismic vulnerability index combines amplification and frequency to assess seismic risk, where higher values mean greater vulnerability.

$$K_g = \frac{{A_0}^2}{f_0} \quad (2)$$

Additionally, sediment thickness (H) can be estimated by

$$H = \frac{V_s}{4f_0} \quad (3)$$

where V_s is the average shear-wave velocity, assuming quarter-wavelength resonance. These parameters are essential for seismic hazard assessment and have been validated in many studies (Lachetl & Bard, 1994; Nakamura, 1989).

2 Methods

The research utilized a combination of field data, geological maps, and software tools to conduct the geophysical analysis. The primary data source was the microtremor measurements collected at 50 points (Figure 1 and 2) in Banyuasin District, South Sumatra. These data were supplemented by geological maps derived from DEMNAS and Inageoportal databases, providing essential contextual information for interpretation.

Microtremor data consisted of ambient seismic noise recordings, which were carefully selected to minimize noise contamination from anthropogenic and natural sources. The selection process involved windowing techniques to isolate signal segments free from transient noise, such as traffic or industrial activity. The flowchart of this research is shown in figure 4.

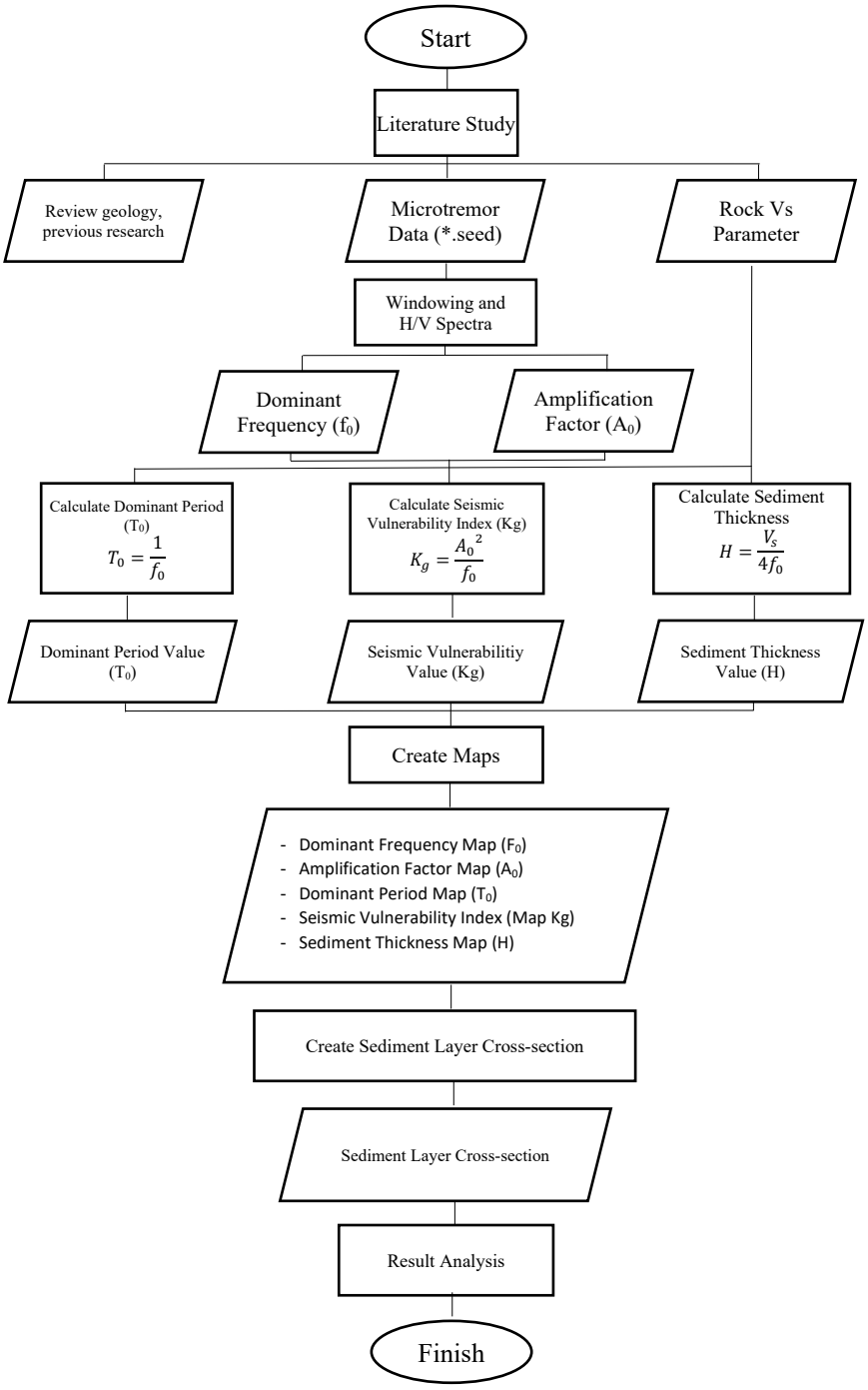

Figure 4. Flowchart.

3 Results

Dominant Frequency Analysis (f_0)

The dominant frequency (f_0), identified as the peak of the HVSR curve, corresponds to the natural vibration frequency of the sediment layer. It reflects the characteristic frequency of the rock layer in a specific area. These frequencies indicate rock type and soil conditions, particularly sediment layer thickness. According to Bard (1999), the dominant frequency is inversely proportional to sediment thickness. Therefore, a low dominant frequency indicates an area with thick sediment or soft soil, while a high dominant frequency indicates an area with a thin sediment layer and harder soil.

The dominant frequency values in Tungkal Jaya District, Musi Banyuasin District, range from 2 to 18 Hz. The dominant frequency values obtained at each measurement point are shown on the dominant frequency distribution map in Figure 5. The dominant frequency is the frequency value that frequently appears in microtremor measurements. It can represent the soil resonance frequency in a given area. Low dominant frequencies are associated with sedimentary soil, whereas high dominant frequencies are associated with hard soil. Lower dominant frequencies correspond to thicker sediment layers. Structural damage caused by earthquakes tends to occur in tall buildings standing on deep sedimentary soil. When the building's dominant frequency approaches or matches the dominant frequency of the soil beneath it, the building's response to seismic waves traveling through the soil medium will be amplified. Dominant frequency is a key parameter in earthquake disaster management, as it influences the response of soil and structures to seismic waves. Based on Kanai's (1983) classification, the average site falls under Type I, characterized by a frequency range from 6.7 Hz to 20 Hz. This frequency range indicates that the area is predominantly covered by a thin layer of sediment.

Amplification Factor Analysis (A_0)

In addition to the dominant frequency (f_0), the amplification factor (A_0) values are also obtained from the processing of the HVSR curve. Seismic wave amplification is characterized by the presence of sedimentary rocks above the bedrock with different densities. This means that if seismic waves propagate through a medium that is softer than the initial medium they passed through, the amplitude will increase.

Surface areas composed of weathered sediments such as clay, sand, peat, and alluvial sand with a hard bedrock have high amplification factor values. This occurs because the impedance contrast between bedrock and sediment is significant in such geological settings. The greater the impedance contrast ratio between these two layers, the higher the amplification factor value.

The amplification factor increases when rock properties are altered by deformation processes such as faulting, folding, and weathering. For the same rock type, the amplification factor can vary depending on the degree of deformation and weathering of the rock body.

The amplification factor is influenced by the shear wave velocity (V_s). The larger the amplification factor, the smaller the shear wave velocity. This is related to the degree of rock compactness, where a decrease in rock compactness will increase the amplification factor value.

In this study, the amplification factor values in the research area, specifically in Tungkal Jaya District, Musi Banyuasin District, range from 1.6 to 5.2. The average amplification factor value is around 2.4 which according to Marijono's (2010) classification, falls into the low category. The amplification factor values obtained at each research point are illustrated in the amplification factor distribution map shown in Figure 6.

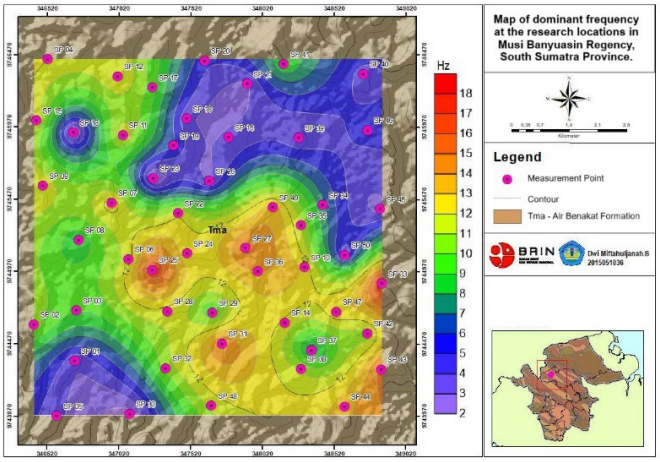

Figure 5. Map of Dominant Frequency.

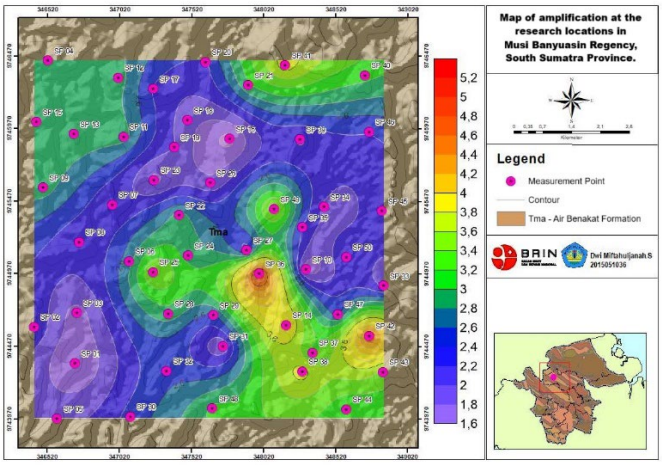

Figure 6. Map of Amplification.

Dominant Period Analysis (T_0)

The dominant period (T_0) is inversely proportional to the dominant frequency, meaning that if the dominant frequency is low, the dominant period of the soil will be correspondingly high. The dominant period represents the fundamental vibration period at which the site or soil layer tends to resonate most strongly when subjected to seismic waves. The dominant period values in the research area are shown in Figure 7.

Based on the distribution map of dominant period values in the research area, the values range from 0.04 to 0.38 seconds. These dominant period values can be used to identify the hardness level of the rock formations present at the research site. Based on the research data and correlated with the soil classifications by Kanai and Omote

Nakajima (Kanai, 1983), the study area consists of soft, medium, and hard soil types. The average dominant period values range from approximately 0.05 to 0.15 seconds, classifying the site as hard rock or Type A. Generally, softer rock formations are associated with increased earthquake vulnerability, whereas harder formations correspond to lower risk. The soil conditions in the study area are predominantly hard rock formations, with some measurement points indicating the presence of soft and medium soil types.

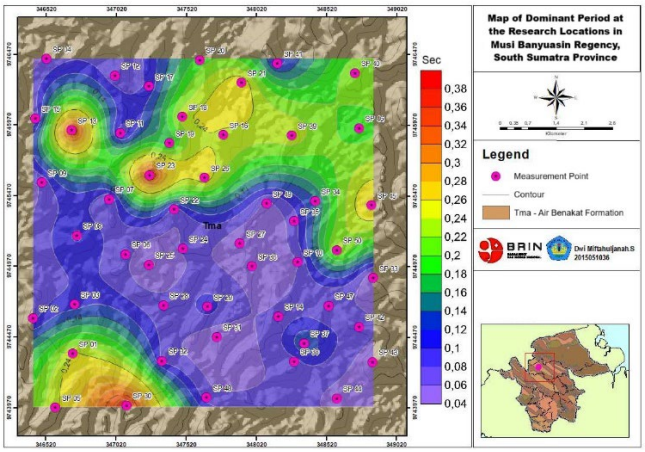

Figure 7. Map of Dominant Period

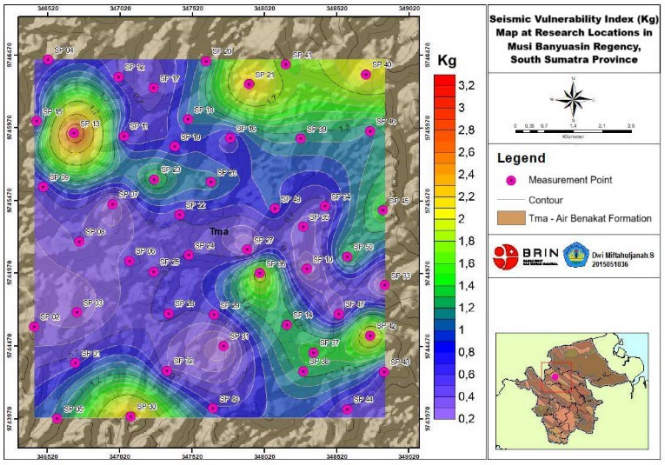

Figure 8. Map of Seismic Vulnerability Index.

Seismic Vulnerability Index (Kg)

The seismic vulnerability index is derived based on the values of dominant frequency and amplification factor. This index analysis indicates the susceptibility of soil caused by seismic waves. The microtremor analysis using the HVSR method shows that the vulnerability index (Kg) in the research area varies between 0.2 and 3.2. The seismic vulnerability index map is shown in Figure 8. The index value is related to the level of vulnerability of an area to earthquake threats and the damage caused by earthquakes. An increased index, reflecting local geological conditions such as low dominant frequency or high amplification factor, corresponds to a higher risk of earthquake damage.

However, as seen in Figure 8, the research area tends to have a low index, which suggests that the sediment layers in the area are relatively thin and lie on a hard layer. Thus, a thin surface sediment layer corresponds to a lower amplification value. Referring to the geological map, the research area consists of materials composed of claystone and sandstone. According to the composition of these rocks, they have relatively low density characteristics because these rock materials tend to have low to moderate water permeability (Sugianto et al., 2016). The denser the rock or the higher its density, the lower the level of building damage, and vice versa. Soft sedimentary rocks amplify earthquake waves, contributing to increased soil vulnerability. When the soil vulnerability index (Kg) is overlaid with the elevation contour map, generally, low soil vulnerability index values are concentrated in areas located on highlands or hilly regions. Areas with a moderate soil vulnerability index value ranging from 3 to 3.2 are found at point SP 13, while other points fall into the low soil vulnerability category. Nakamura also reported in his research in the Marina district of San Francisco that areas experiencing severe damage had alluvial geological conditions, specifically coastal regions with high seismic vulnerability index values (Nakamura, 2000). The seismic vulnerability index decreases as one moves into hilly areas characterized by harder rock structures and thinner sediment layers, resulting in less severe damage caused by earthquakes.

Sediment Layer Thickness Analysis (H)

The sediment layer is a layer formed from the processes of weathering and deposition. The materials in this layer are prone to deformation or mass movement, so when the weight of the material increases due to water absorption up to the impermeable layer (bedrock), it will cause material movement. The thickness of the sediment layer is determined based on the measured dominant frequency and the shear wave velocity at the ground surface. It is then calculated using equation 3. Mathematically, the sediment layer thickness is inversely proportional to the dominant frequency. From Figure 9, the research area, based on its response to earthquakes, can be estimated such that when the sediment layer has a low value, it correlates with a high dominant frequency and the resulting amplitude will be smaller, and vice versa. This also affects the soil vulnerability in the research area, making it a region that is not prone to earthquakes. Based on the calculation results, the sediment layer thickness (H) in the research area ranges from 8 to 64 meters.

Sediment Thickness Profile by Depth

In the cross-section (Figure 10 a), the soft sediment layer is marked in yellow, located between 15 and 50 meters below the ground surface. This soft sediment layer is interspersed with a bedrock or hard layer marked in gray, appearing approximately 15 meters below the soft layer. A red line separates these two layers, indicating the transition between different geological materials.

Figure 10 (b) shows a contour map representing surface elevation at the measurement area. Red/orange colors indicate higher elevations, while blue indicates lower elevations. Contour lines provide detailed elevation changes across the area. Figure 10 (c) shows a contour map of sediment thickness

beneath the surface. Red/orange colors indicate thicker sediment layers, while blue indicates thinner layers. Contour lines highlight thickness variations at different points.

From the vertical cross-section, it can be identified that the soft sediment layer (Soft) lies above the bedrock or hard layer (Hard).

This soft sediment layer is most likely composed of less dense material that is more easily deformed. By examining the elevation contour map and sediment thickness map, the relationship between

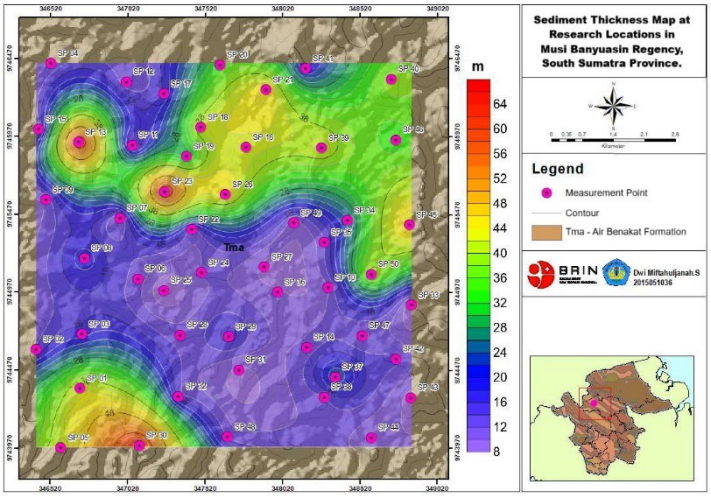

Figure 9. Sediment Thickness Map.

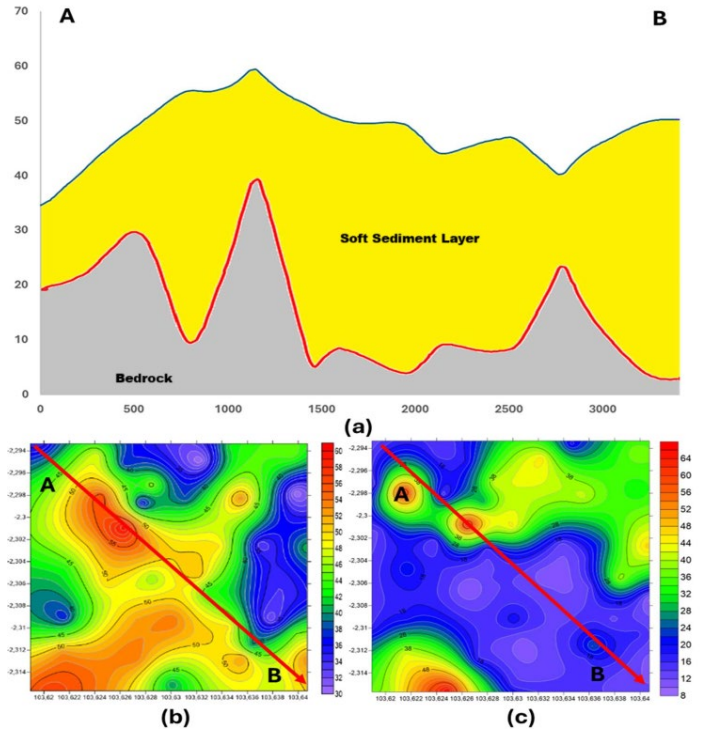

Figure 10. (a) Cross-section of the soft sediment layer thickness along Line 1 (b) Topographic contour of measurement points (c) Contour map of the soft sediment layer thickness.

surface topography and sediment thickness distribution can be understood.

In the study area, regions of higher elevation are generally characterized by thinner sediment layers, while lower elevation zones exhibit thicker sediment deposits. The vertical cross-section delineates the boundary between the soft sediment layer and the underlying hard rock formation. Additionally, the elevation and sediment thickness contour maps provide comprehensive visualizations of the area's topographic variability and sediment distribution.

Figure 11(a) shows a detailed vertical cross-section of two subsurface layers, separated by a red line that marks the boundary between the yellow-shaded soft sediment and the gray bedrock beneath. The thickness of the soft sediment layer exhibits spatial variability, ranging approximately from 10 to 45 meters. The bedrock layer is observed to begin at depths roughly 10 meters below the base of the soft sediment layer. Figure 11(b) depicts a contour map of surface elevation, where

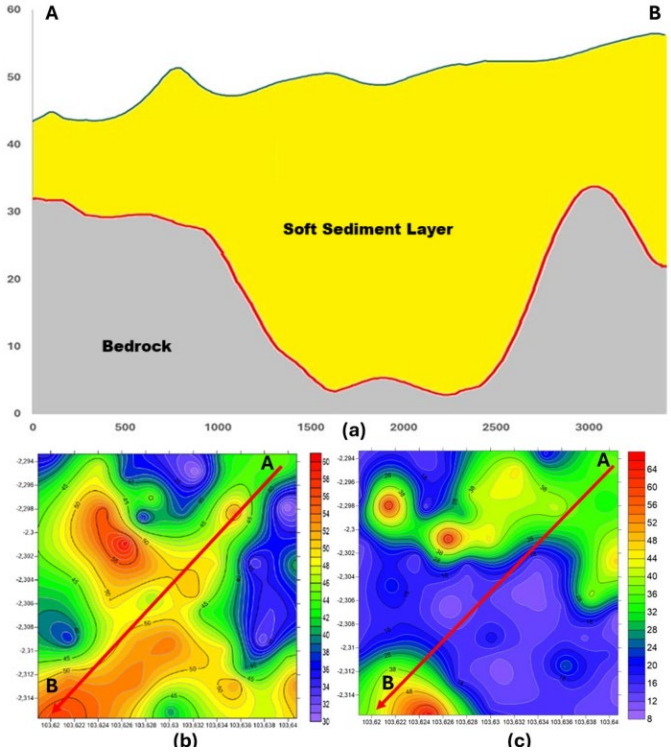

Figure 11. (a) Cross-section of the soft sediment layer thickness along Line 2 (b) Topographic contour of measurement points (c) Contour map of the soft sediment layer thickness.

red hues correspond to higher elevations and blue hues indicate lower elevations. Points A and B are marked on this map and connected by a red line, which corresponds to the cross-sectional profile shown in Figure 11(a). Similarly, Figure 11(c) illustrates a contour map of sediment thickness, with red areas indicating thicker sediment deposits and blue areas representing thinner layers. The same points A and B are connected by a red line, facilitating direct comparison across all three figures. The Horizontal-to-Vertical Spectral Ratio

(HVSR) method was applied to characterize subsurface soil properties through the analysis of seismic wave spectral ratios. Analysis of the transect between points A and B reveals a strong spatial correlation between sediment thickness and surface elevation. Variations in sediment thickness closely align with elevation changes, indicating a strong link between surface geomorphology and subsurface sediment distribution.

Figure 12(a) shows a cross-section of two soil layers, with a red line marking the boundary between the soft upper sediment (yellow) and the underlying hard bedrock (gray). The soft layer is colored yellow, while the hard layer is gray, with variations in the thickness of the soft layer at different points indicating heterogeneity. In profile four, it can be observed that the soft layer extends from 0 to 45 meters below the ground surface. The soft layer is also interspersed with hard layers that begin to appear at approximately 0 meters below the soft layer.

The second image (b) is an elevation contour map showing height variations, where red indicates higher elevations and blue indicates lower elevations. Points A and B on this map are connected by the same red line as points A and B on the layer cross-section.

The third image (c) shows a contour map of sediment layer thickness, with color variations representing differences in thickness: red indicates thicker sediment layers, and blue indicates thinner layers. Points A and B also appear on this map, connected by the same red line as in the previous images. The layer cross-section reveals two main layers: a soft sediment layer above a hard layer, which is likely bedrock. The varying thickness of the soft layer indicates differences in composition and material properties beneath the surface. The elevation contour map shows the surface topography of the measured area, with significant elevation variations indicating height differences across the region.

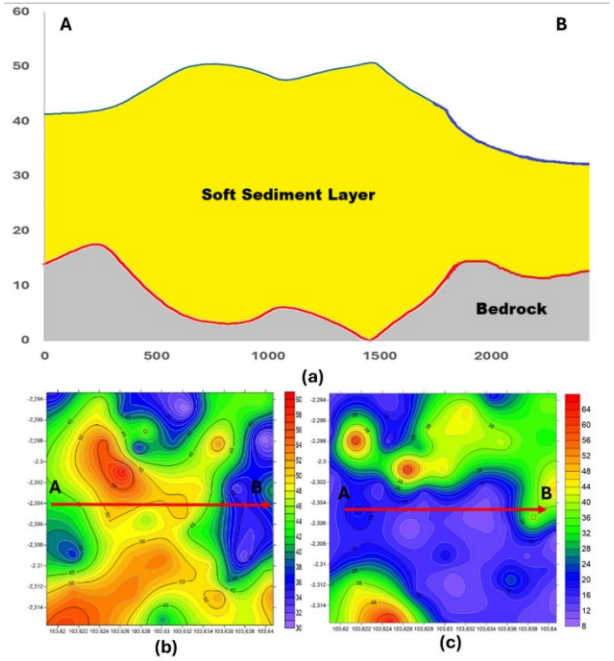

Figure 12. (a) Cross-section of the soft sediment layer thickness along Line 3 (b) Topographic contour of measurement points (c) Contour map of the soft sediment layer thickness.

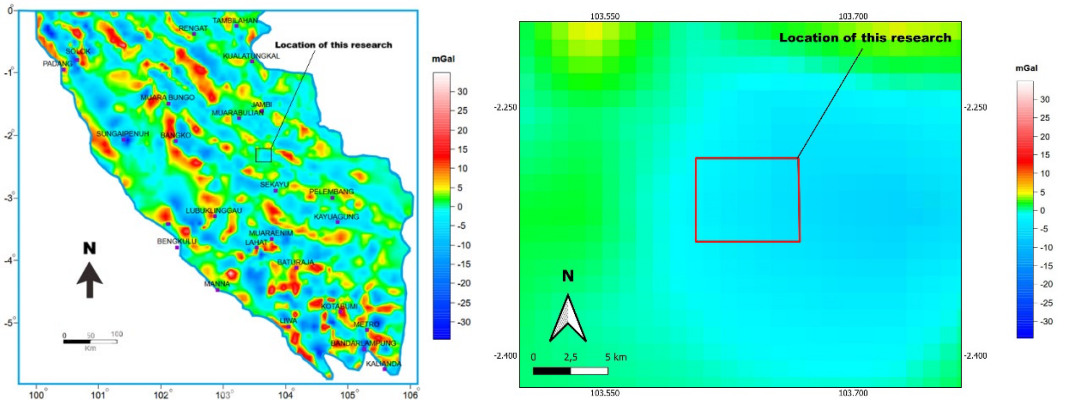

Figure 13. (a) Residual Gravity Anomaly Map (b) Zoomed-in section of our research area (Setiadi et al., 2010).

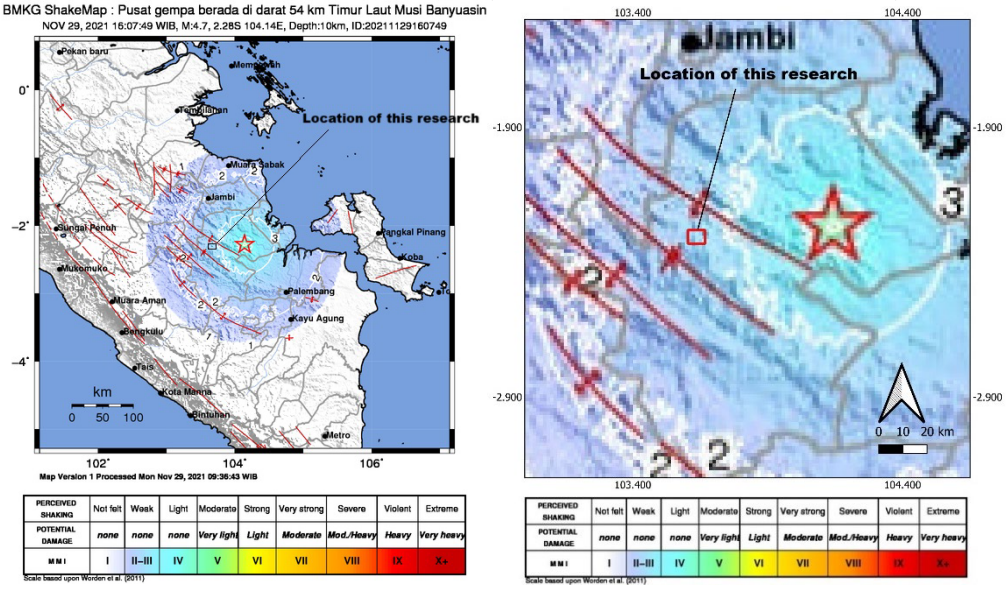

Figure 14. (a) Shakemap of the Musi Banyuasin Earthquake on Monday, 29 November 2021 (M4.7, Depth 10 km) (b) Zoomed-in section of our research area (BMKG, 2021).

The sediment thickness contour map illustrates variations in the thickness of the soft sediment layer above the hard layer, with red areas indicating greater thickness and blue areas indicating thinner thickness. The relationship between points A and B across all images demonstrates how the thickness of the soft sediment layer changes along this line, which be related to the topographic variations.

4 Discussion

Based on the analysis and findings of Maringue et al. (2021), a significant relationship exists between the dominant period (T_0) and residual gravity anomalies within the study area. Residual gravity anomalies, shown in Figure (13) range from 0 – 5 mGal, which smooth local variations and helps explain observed spatial heterogeneity. The dominant period values vary between 0.04 and 0.38 seconds. This regional-scale calculation inherently smooths localized variations, which explains some spatial heterogeneity observed in the data. A notable inverse relationship is observed as the dominant period increases, the residual gravity

anomaly becomes more negative. This trend is geophysically consistent, as higher dominant periods typically indicate thicker or softer sediment layers with lower densities, which correspond to stronger negative gravity anomalies. Spatially, within the delineated black rectangular area, residual gravity anomalies exhibit an increasing negative trend toward the east, which closely parallels the corresponding increase in dominant period (T_0) values, particularly in the northern sector. In contrast, the southern sector shows smaller dominant period values but displays a similar eastward trend of increasingly negative residual gravity anomalies. This pattern result from the limited spatial resolution of the residual gravity anomaly data, which were processed at a regional scale and thus lack detailed representation of localized variations. Despite this limitation, the observed spatial correlation strongly supports the conclusion that dominant period and residual gravity anomalies are interrelated parameters, offering valuable insights into the subsurface geophysical characteristics of the study region.

Furthermore, the shakemap for the earthquake event in Musi Banyuasin (Figure 14) indicates that the affected area experienced shaking levels corresponding to only 2 to 3 on the Modified Mercalli Intensity (MMI) scale. According to this scale, the perceived shaking is classified as weak, with no potential for significant damage. The seismic vulnerability index serves as a complementary parameter that effectively correlates with the MMI scale, providing a quantitative measure of the area's susceptibility to earthquake-induced damage. The results show that the seismic vulnerability index values range from 0.2 to 3.2, with an average value of approximately 0.3. These low values align well with the shakemap data, reinforcing the conclusion that the region generally experiences lower earthquake shaking compared to areas with a high seismic vulnerability index. This phenomenon is similar to the findings of Akkaya (2020) research in Turkey, which showed that regions with high seismic vulnerability tend to have buildings with higher damage. The correlation between the seismic vulnerability index and the shakemap highlights the index's usefulness in validating and improving seismic hazard assessments by linking ground shaking intensity with the vulnerability of local structures and soils.

5 Conclusions

Residual gravity anomalies (0–5 mGal) show a clear inverse correlation with dominant period (T_0). Areas in the eastern sector exhibit more negative gravity values alongside higher T_0, consistent with thicker, less dense sediments. Statistical analysis confirms this relationship (Pearson $r = -0.68$, $R^2 = 0.46$), supporting the link between sediment thickness and gravity lows. However, regional smoothing of gravity data reduces resolution and may mask small-scale heterogeneities.

The seismic vulnerability index (K_g) ranges from 0.2 to 3.2, with low values dominating most of the district. These values align with BMKG shakemap data for the 2021 M4.7 event, which showed Modified Mercalli Intensity (MMI) II–III. This suggests generally weak shaking and low damage potential. Yet, low K_g does not guarantee safety if buildings have poor structural quality or do not comply with seismic codes. Regions in the central sector with

moderate K_g values highlight areas where building standards must be reinforced.

Overall, spatial patterns indicate that the western sector is characterized by thicker sediments and lower f0, while the eastern sector has thinner sediments and higher f0. This spatial heterogeneity is essential for site-specific planning and seismic microzonation.

References

Abdelrahman, K., Al-Otaibi, N., Ibrahim, E., & Binsadoon, A. (2021). Landslide susceptibility assessment and their disastrous impact on Makkah Al-Mukarramah urban Expansion, Saudi Arabia, using microtremor measurements. *Journal of King Saud University - Science*, *33*(5), 101450. https://doi.org/https://doi.org/10.1016/j.jksus.2021.101450

Akkaya, İ. (2020). Availability of seismic vulnerability index (Kg) in the assessment of building damage in Van, Eastern Turkey. *Earthquake Engineering and Engineering Vibration*, *19*(1), 189–204. https://doi.org/10.1007/s11803-020-0556-z

Barber, A. J., Crow, M. J., & Milsom, J. S. (Eds.). (2005). *Sumatra: Geology, Resources and Tectonic Evolution*. Geological Society of London. https://doi.org/10.1144/GSL.MEM.2005.031

Bard, P.-Y. (1999). Microtremor measurements: A tool for site effect estimation? *Conference: Second International Symposium on the Effects of Surface Geology on Seismic MotionAt: Yokohama, JapanVolume: Irikura, Kudo, Okada & Sasatani, (Eds), Balkema*, 1251–1279.

BMKG. (2021). *BMKG ShakeMap : Pusat gempa berada di darat 54 km Timur Laut Musi Banyuasin*. Pusat Seismologi Teknik Geofisika Potensial Dan Tanda Waktu. https://simora.bmkg.go.id/simora/web/page/shakemap_terkini

Hadi, A. I., Farid, M., Refrizon, R., Harlianto, B., Hudayat, N., & Krisbudianto, M. (2021). Mapping of Earthquake Vulnerability Potential in Bengkulu City Using Microtremor Data and Analytical Hierarchy Process Method. *Jurnal Fisika Flux: Jurnal Ilmiah Fisika FMIPA Universitas Lambung Mangkurat*, *18*(2), 105–118.

Hadi, A. I., Harlianto, B., Hudayat, N., Farid, M., Virgo, F., Fadli, D. I., & Humairah, F. (2025). Micro-Zonation Mapping of Landslide Potential Using Statistical Weighting Method of Analytical Hierarchy Process (AHP) in South Bengkulu–Lahat Road for Disaster Mitigation. *Journal of Research in Science Education*, *11*(2), 880–889.

Hakimi, B., Masoumi, Z., Ghods, A., & Etemad-Saeed, N. (2019). Microtremor HVSR Study of Site Effects in Zanjan City (Iran). *Iranian Journal of Geophysics*, *12*(4), 115–139. https://www.ijgeophysics.ir/article_82770.html

Hardy, T., Hakim, A. R., Rohadi, S., Prayogo, A. S., Ngadmanto, D., Susilanto, P., Rasmid, Sunardi, B., Pakpahan, S., Setyonegoro, W., Kurniawan, T., Nugraha, J., Perdana, Y. H., Setiadi, T. A. P., Sulastri, Rahman, A., Vita, A. N., Priyobudi, Martha, A. A., … Yuliatmoko, R. S. (2021). Development Prototype of Indonesia Seismic Microzonation Information System (Inasmis). *IOP Conference Series: Earth and Environmental Science*, *873*(1), 12035. https://doi.org/10.1088/1755-1315/873/1/012035

Irsyam, M., Sengara, I. W., Aldiamar, F., Widiyantoro, S., Triyoso, W., Natawidjaja, D. H., Kertapati, E., Meilano, I., Asrurifak, M., & Ridwan, M. (2010). *Summary of the Results of the Indonesia Earthquake Map Revision Team Study 2010.* KemenPU.

Kanai, K. (1983). Engineering seismology. *Earthquake Engineering & Structural Dynamics*, *11*(5), 727–728. https://doi.org/https://doi.org/10.1002/eqe.4290110511

Lachetl, C., & Bard, P.-Y. (1994). Numerical and Theoretical Investigations on the Possibilities and Limitations of Nakamura's Technique. *Journal of Physics of the Earth*, *42*(5), 377–397. https://doi.org/10.4294/jpe1952.42.377

Lovett, R. A. (2006). *Deadly Java Quake Highlights "Ring of Fire" Dangers*. National Geographic News. http://news.nationalgeographic.com/news/2006/05/060530-java-quake.html

Ma, H., & Liao, B.-Y. (2024). Study on Site Effect in Nanning City Using HVSR Method. *Civil Engineering and Architecture*, *12*(2), 1165–1179. https://doi.org/10.13189/cea.2024.120235.

Marijono. (2010). *Estimation of Soil Dynamic Characteristics from Microtremor Data*

Bandung Area. Bandung Insitute of Technology.

Maringue, J., Sáez, E., & Yañez, G. (2021). An Empirical Correlation between the Residual Gravity Anomaly and the H/V Predominant Period in Urban Areas and Its Dependence on Geology in Andean Forearc Basins. In *Applied Sciences* (Vol. 11, Issue 20). https://doi.org/10.3390/app11209462

Maulidah, D. F., & Santosa, B. J. (2016). Analysis of Seismicity Distribution in South Sumatra Region Using the Double Difference Method. *JURNAL SAINS DAN SENI ITS*, *5*(2), 54–58.

Miezah-Adams, M., Torvor, F. K., Ansah, E., Ewusi, A., & Boateng, E. K. (2024). *Microtremor HVSR Technique for Seismic Risk Vulnerability Studies and Microzonation of Site Materials* (M. Mokhtari (Ed.)). IntechOpen. https://doi.org/10.5772/intechopen.1006526

Minardi, S., Ardianto, T., Alaydrus, A. T., Tawakal, M. I., & Martha, A. A. (2023). Investigation of Sediment Thickness Beneath The Mandalika Circuit and Its Surroundings based on Microtremor Data. *International Journal of GEOMATE*, *25*(112), 40–47. https://doi.org/https://doi.org/10.21660/2023.112.4108

Nakamura, Y. (1989). A method for dynamic characteristics estimation of subsurface using microtremor on the ground surface. *Railway Technical Research Institute*, *30*(1).

Nakamura, Y. (2000). Clear Identification of Fundamental Idea of Nakamura's Technique and Its Applications. *The 12th World Conference on Earthquake Engineering*.

Salama, A., Moussa, H. H., & Maklad, M. (2024). An earthquake spectra parameters near the new capital administrative city, Egypt. *Discover Civil Engineering*, *1*(1), 22. https://doi.org/10.1007/s44290-024-00026-6

Setiadi, I., Setyanta, B., & Widijono, B. S. (2010). Delineation of South Sumatra Sedimentary Basins Based on Gravity Data Analysis. *Journal of Geology and Mineral Resources*, *20*(2), 93–106. https://doi.org/https://doi.org/10.33332/jgsm.geologi.v20i2.164

Sugianto, N., Farid, M., & Suryanto, W. (2016). Local Geology Condition of Bengkulu City Based on Seismic Vulnerability Index (Kg). *ARPN Journal of Engineering and Applied Sciences*, *11*(7), 4797–4803.

Supartoyo, S., & Abdurahman. (2008). *Indonesia's Destructive Earthquake Events 2007*. Badan Geologi.

Susilawati, R., & Ward, C. R. (2006). Metamorphism of mineral matter in coal from the Bukit Asam deposit, south Sumatra, Indonesia. *International Journal of Coal Geology*, *68*(3), 171–195. https://doi.org/https://doi.org/10.1016/j.coal.2006.02.003

Takai, & Tanaka. (1961). On microtremor VIII. *Bull. Earthquake Res. Inst*, *39*, 97–114.

Tawakal, M. I., Haris, A., & Martha, A. A. (2020). Estimating shear wave velocity (Vs30) of East Java, Indonesia, using ambient noise inversion of horizontal to vertical spectral ratio (HVSR). *IOP Conference Series: Earth and Environmental Science*, *538*(1), 12012. https://doi.org/10.1088/1755-1315/538/1/012012

Widia Pamungkas Isburhan, R., Nuraeni, G., Verdhora Ry, R., Yudistira, T., Cipta, A., & Cummins, P. (2019). Horizontal-to-Vertical Spectral Ratio (HVSR) Method for Earthquake Risk Determination of Jakarta City with Microtremor Data. *IOP Conference Series: Earth and Environmental Science*, *318*(1), 12033. https://doi.org/10.1088/1755-1315/318/1/012033

Zavala, N., Clemente-Chávez, A., Figueroa-Soto, Á., González-Martínez, M., & Sawires, R. (2021). Application of horizontal to Vertical Spectral Ratio microtremor technique in the analysis of site effects and structural response of buildings in Querétaro city, Mexico. *Journal of South American Earth Sciences*, *108*, 103211. https://doi.org/https://doi.org/10.1016/j.jsames.2021.103211.